

TXS 1433+205: The most distant gamma-ray emitting FR II radio galaxy

Vaidehi S. Paliya,^{1*} D. J. Saikia¹ and C. S. Stalin,²

¹*Inter-University Centre for Astronomy and Astrophysics (IUCAA), SPPU Campus, Pune 411007, India*

²*Indian Institute of Astrophysics, Block II, Koramangala, Bengaluru 560034, Karnataka, India*

Accepted XXX. Received YYY; in original form ZZZ

ABSTRACT

The orientation of the jet axis to the line of sight of the observer plays a major role in explaining the phenomena observed from blazars and radio galaxies. In the γ -ray band, only a handful of radio galaxies have been identified, all being located in the nearby Universe ($z < 0.5$). Here we report the identification of 4FGL J1435.5+2021, associated with TXS 1433+205, as a Fanaroff-Riley type II (FR II) radio galaxy at a considerably higher redshift of $z = 0.748$, thereby making it the most distant γ -ray detected radio galaxy known as of now. The Very Large Array Sky Survey data at 3 GHz resolves the source morphology into a bright core, a jet and two hotspots, with a total end-to-end projected length between lobe extremities of ~ 170 kpc. The optical and radio properties of this enigmatic object suggest it to be a high-excitation FR II radio galaxy. The multi-wavelength behaviour of TXS 1433+205 is found to be similar to other γ -ray detected FR II sources but is at the high luminosity end. We suggest that the ongoing and upcoming high-resolution radio surveys will lead to the identification of many more high-redshift radio galaxies in the γ -ray sky, thus allowing comprehensive studies of misaligned relativistic jets.

Key words: galaxies: jets – gamma-rays: galaxies – BL Lacertae objects: general

1 INTRODUCTION

The extragalactic γ -ray sky as observed by *Fermi*-Large Area Telescope (LAT) is dominated by active galactic nuclei (AGN) hosting beamed relativistic jets, i.e., blazars. Though in small numbers, *Fermi*-LAT has also detected significant γ -ray emission from AGN with misaligned jets, mainly radio galaxies (cf. Ajello et al. 2020). These are relatively γ -ray faint sources likely due to less extreme Doppler boosting. Nevertheless, they are being extensively studied and surveys are being intensively searched to identify new γ -ray emitters to study the radiative processes powering relativistic jets and, in general, AGN unification (see, e.g., Kataoka et al. 2011; Grandi et al. 2012; Paliya 2021). Based on the radio morphology and power, radio galaxies have been further divided as faint edge-darkened Fanaroff-Riley type I (FR I) and luminous edge-brightened FR II sources usually showing bright hotspots (Fanaroff & Riley 1974). More FR Is have been detected with the *Fermi*-LAT compared to the FR II ones (cf. Ajello et al. 2020). This could be possibly due to the relatively flat γ -ray spectra of the former and/or their closer proximity compared to FR IIs (cf. Fukazawa et al. 2022) but it is yet to be fully understood.

Gamma-ray emitting radio galaxies have mostly been found in the low-redshift Universe ($z < 0.5$, Abdo et al. 2010; Chiaro et al. 2020). For example, in the second data release of the fourth catalog of the *Fermi*-LAT detected AGN (4LAC-DR2 Ajello et al. 2020), the farthest known radio galaxy is 3C 17 at $z = 0.22$. Recently, Bruni et al. (2022) have identified an FR II radio galaxy, IGR J18249–3243, at $z = 0.36$ among the unclassified γ -ray sources listed in the 4LAC catalog. Identifying γ -ray emitting radio galaxies at high redshifts is crucial not only to find the most γ -ray luminous members of this class

and constrain their evolution (e.g., Fukazawa et al. 2022) but also to understand the radiative mechanisms, e.g., leptonic versus hadronic, responsible for the observed high-energy emission. Indeed, radio galaxies have been proposed as a plausible source of cosmic neutrinos detected with the IceCube observatory (Hooper 2016) indicating hadronic processes may power their radio jets.

In this Letter, we present the identification and multi-frequency properties of the γ -ray detected object 4FGL J1435.5+2021, associated with the radio source TXS 1433+205 (bayesian association probability ≈ 0.99 , Ajello et al. 2020), as the most distant (as of now) γ -ray emitting FR II radio galaxy at $z = 0.748$, revealed by the ongoing Very Large Array Sky Survey (VLASS, Lacy et al. 2020). This object has been misclassified as a BL Lac in the 4LAC-DR2 catalog though we show that its multi-frequency properties resemble well that of γ -ray detected FR II radio galaxies. We adopt a flat cosmology with $H_0 = 70 \text{ km s}^{-1} \text{ Mpc}^{-1}$ and $\Omega_M = 0.3$. At the redshift of $z = 0.748$, 1 arcsec = 7.33 kpc.

2 RADIO CHARACTERIZATION

TXS 1433+205 lies in the footprint of several radio surveys, e.g., NRAO VLA Sky Survey (NVSS, Condon et al. 1998, 1.4 GHz), Faint Images of the Radio Sky at Twenty-Centimeters (FIRST, White et al. 1997, 1.4 GHz), the Galactic and extragalactic all-sky MWA survey (Wayth et al. 2015, 74–231 MHz), and in the TIFR GMRT Sky Survey (TGSS, Intema et al. 2017, 150 MHz). However, none of these surveys, except FIRST, could resolve the source morphology. Even in the FIRST image, at 5 arcsec resolution, TXS 1433+205 is marginally resolved. Between 1.4–5 GHz frequencies, the object has a flat radio spectrum ($\alpha = -0.48$, $S_\nu \propto \nu^\alpha$, Healey et al. 2007). On the other hand, considering the flux densities at 8.4 GHz and 150

* E-mail: vaidehi.s.paliya@gmail.com (VSP)

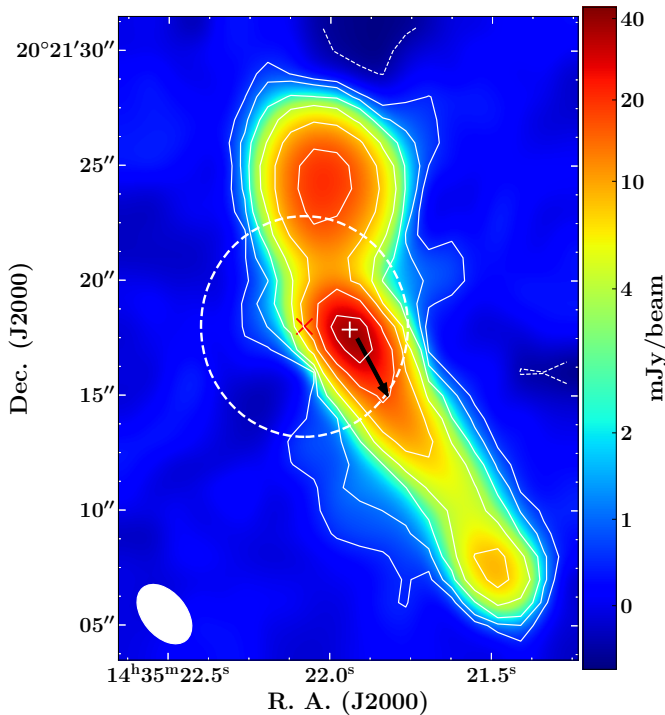


Figure 1. VLASS (3 GHz) image of TXS 1433+205. The rms is 0.17 mJy per beam and contours are $3 \times \text{rms} \times (-1, 1, 2, 4, 8, 16, 32, 64)$. The ‘X’ mark represents the X-ray core position measured by *Swift*-XRT and the dashed circle refers to the uncertainty in the optimized position at 90% confidence. The ‘+’ mark shows the VLBI core position and the black arrow highlights the direction of the boosted jet. North is up and east to the left.

MHz, the overall radio spectrum is steep ($\alpha = -0.78$). The 150 MHz luminosity of the source is $\approx 5 \times 10^{27} \text{ W Hz}^{-1}$, well above the FR I/II threshold.

VLASS is an ongoing radio survey at 2–4 GHz with high angular resolution (~ 2.5 arcsec) and sensitivity (0.12 mJy per beam for the first VLASS epoch). We browsed the VLASS quick look images¹ of TXS 1433+205 and found a resolved radio morphology. As can be seen in Figure 1, the object is resolved into three components besides the extended radio jet: a central core and two lobes with hotspots. These radio observations, along with the optical (Section 3) and multi-wavelength (Section 4) observations, unambiguously confirm that TXS 1433+205 is a γ -ray emitting FR II radio galaxy. The radio core of the object is positionally consistent with a moderately bright X-ray source detected with the *Swift* X-ray Telescope (XRT, observed $F_{0.3-10 \text{ keV}} \sim 3 \times 10^{-13} \text{ erg cm}^{-2} \text{ s}^{-1}$). The north radio lobe ends at ~ 10 arcsec (projected length ~ 73 kpc) far from the core, whereas, the south-west lobe at a distance of ~ 14 arcsec (projected length ~ 104 kpc).

The flux density of the core is comparable to that of the northern lobe, 57.7 ± 0.4 mJy, and 67.2 ± 0.6 mJy, respectively, whereas the south-western lobe is considerably fainter with a flux density of 12.8 ± 0.4 mJy. The peak flux densities of the northern and south-western hotspots are 21.3 ± 0.2 mJy/beam and 10.3 ± 0.2 mJy/beam, respectively. The Laing-Garrington effect clearly demonstrated that

the apparent asymmetry of jets in radio-loud AGN is due to relativistic beaming with the prominent jet approaching us (Garrington et al. 1988; Laing 1988). Hence the hotspot and lobe facing the jet is also on the approaching side and usually tends to be brighter than the one on the opposite side, possibly due to mild relativistic beaming of the hotspots (e.g. Garrington et al. 1991). In the case of TXS 1433+205, a nuclear Very long baseline interferometry (VLBI)-scale jet is also seen to point in a similar direction as the large-scale jet. The VLBI image taken in the X-band (Petrov 2021) is shown in the appendix (Figure A1). The considerably fainter hotspot and lobe on its south-western side, which face the jet and hence are on the approaching side, suggest significant dissipation of energy in the jet. Several such examples are known in the literature (for a review see e.g. Saikia 2022). Furthermore, we compute the core dominance (C_D) following Abdo et al. (2010). It is determined as $C_D = \log(F_{\text{core}}/(F_{\text{tot}} - F_{\text{core}}))$, where $F_{\text{tot/core}}$ is the total/core flux density in the source rest-frame at 3 GHz. This parameter allows us to constrain the viewing angle of the jet since $F_{\text{core}} \propto \delta^{3+\alpha}$ (δ is the Doppler factor, cf. Dermer 1995) whereas the lobe emission is expected to be largely isotropic and hence unbeamed. For TXS 1433+205, we get $C_D = -0.11$ which is similar to other γ -ray detected FR I and II radio galaxies (Abdo et al. 2010). This indicates a relatively small viewing angle of the jet. Indeed, large core dominance hints that AGNs viewed closer to the jet axis have a higher probability to be detected with the *Fermi*-LAT.

Recently, Pajdosz-Śmierciak et al. (2022) have reported the identification of seven blazars with extended jet morphologies similar to radio galaxies using MHz frequency observations taken with the Low-Frequency Array (LOFAR). The change in the direction of the jet out of the sky plane possibly due to some kind of precession mechanism may lead to the observation of extended radio emission revealing the older AGN activity as proposed by Pajdosz-Śmierciak et al. (2022). The LOFAR observations taken at 144 MHz probably trace the old/previous AGN phase since the high-energy electrons emitting GHz frequency radiation cool faster than those radiating MHz frequency emission. Since TXS 1433+205 exhibits bi-polar extended emission at GHz frequencies as observed by VLASS and a normal low-frequency spectral index of -0.78 , it probably represents the current jet activity. The overall structure appears misaligned which is supported by the fact that the Northern lobe lies on a different axis with respect to the one connecting the core and Southern lobe. This could also be due to interaction with the inter-galactic medium, which could contribute to its shorter distance from the core, and the stronger flux density². It is not covered in the second data release of the LOFAR survey (Shimwell et al. 2022) and is not resolved in the 888 MHz observations taken with the Rapid ASKAP Continuum Survey (RACS, McConnell et al. 2020). High-resolution, low-frequency MHz observations of TXS 1433+205 will be required to reveal the episodic AGN activity, if any.

3 OPTICAL SPECTROSCOPIC CLASSIFICATION

The optical spectrum of TXS 1433+205 was first published by Hook et al. (1996) and found to be featureless. This may have led to its classification as a BL Lac object (Véron-Cetty & Véron 2010). However, better quality spectra taken with the Sloan Digital Sky Survey (SDSS, Figure 2, top panel) revealed the presence of strong $[\text{O III}]\lambda 3727$ and $[\text{O III}]\lambda 5007$ emission lines securing the source

¹ <https://science.nrao.edu/vlass/data-access/vlass-epoch-1-quick-look-users-guide>

² Part of the misalignment could be due to projection effects as the source is viewed at a relatively small angle to the line of sight, although not head-on.

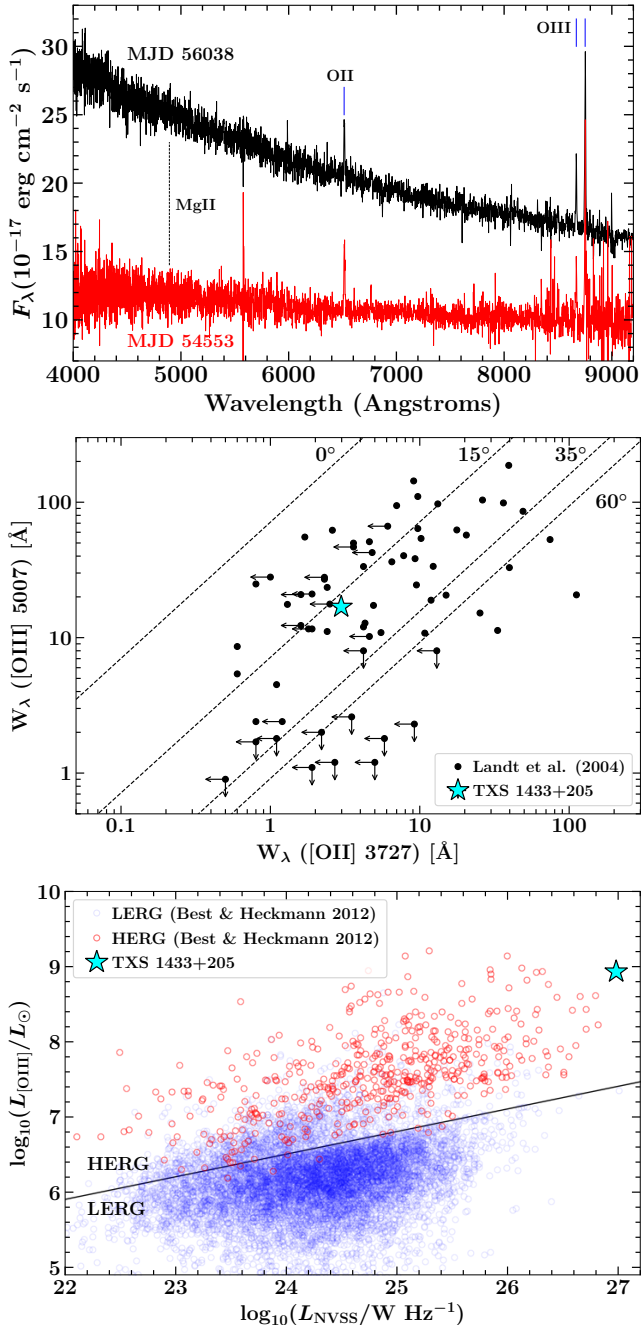


Figure 2. Top: The SDSS optical spectrum of TXS 1433+205. Prominent emission/absorption features are marked. Middle: This plot shows the position of TXS 1433+205 in the [O II] λ 3727 and [O III] λ 5007 EW plane. The shown lines, highlighting the jet viewing angles, and other jetted sources (black circles) are adopted from Landt et al. (2004). Bottom: The location of TXS 1433+205 in the [O III] emission line luminosity versus radio luminosity diagram. The solid line indicates an approximate divide between HERGs and LERGs proposed by Best & Heckman (2012).

redshift as $z = 0.748$. This rules out the BL Lac classification of the source. Recently, Foschini et al. (2022) have also updated the classification of TXS 1433+205 as a misaligned AGN based on the observation of [O II] λ 3727 and [O III] λ 5007 emission lines and steep radio spectrum as also found by us. Interestingly, SDSS spectra taken at two different epochs show ‘bluer-when-brighter’ flux variations

which can be explained due to the non-negligible contamination by the jet. The low-activity state spectrum, on the other hand, hints for the presence of broad Mg II and H β emission lines although the signal-to-noise ratio of the data is poor³.

Landt et al. (2004) proposed that beamed AGN and radio galaxies can be separated on the [O II] λ 3727–[O III] λ 5007 equivalent width (EW) plane, thus constraining the viewing angle of the jet. This is because the line radiation is expected to be isotropic and the AGN continuum and jet contamination vary with the viewing angle, hence the line EWs as well (see also, Risaliti et al. 2011). Since both [O II] λ 3727 and [O III] λ 5007 lines are strong, we directly use the EW measured by the SDSS pipeline (Ahumada et al. 2020) and found it to be $2.98 \pm 0.30 \text{ \AA}$ and $16.87 \pm 0.61 \text{ \AA}$, respectively. In Figure 2 (middle panel), we show the position of TXS 1433+205 in the line EW diagram (Landt et al. 2004) and estimate the viewing angle to be $\sim 15^\circ$. The presence of such a moderately misaligned jet is supported by the γ -ray detection and flux variability seen in the SDSS spectrum.

To determine whether TXS 1433+205 belongs to the class of the high-excitation or low-excitation radio galaxies (HERG and LERG, respectively), we highlight its position in the radio–[O III] λ 5007 luminosity diagram (Figure 2, bottom panel). For comparison, we also show the galaxies studied by Best & Heckman (2012) and their proposed HERG/LERG divide. In this diagram, TXS 1433+205 lies in a region mainly populated by HERGs and well above the HERG/LERG division line which indicates a radiatively efficiently accretion (accretion rate $> 1\%$ of the Eddington rate, Best & Heckman 2012) powering the system. A large EW ($> 3 \text{ \AA}$) of the [O III] λ 5007 line also supports the HERG classification of the source (Jackson & Rawlings 1997; Buttiglione et al. 2009).

4 MULTI-WAVELENGTH PROPERTIES

The top left panel of Figure 3 shows the broadband spectral energy distribution (SED) of TXS 1433+205. For comparison, we also plot the SEDs of 42 *Fermi*-LAT detected FR I and II sources (Ajello et al. 2020; Fukazawa et al. 2022) using the data taken from the Space Science Data Center SED builder tool⁴. A quick look at this plot suggests TXS 1433+205 to be among the most luminous γ -ray detected radio galaxies. In particular, this object is the most luminous in the radio and γ -ray bands as can be seen in Figure 3 (top right panel). Compared to blazars, the 0.1–100 GeV isotropic γ -ray luminosity of TXS 1433+205 is similar to the low-luminosity flat spectrum radio quasars but is on the higher side of that for BL Lac objects (Figure 3, bottom left panel). The γ -ray spectrum of the source (photon index $\Gamma_\gamma = 2.17 \pm 0.09$) appears harder in comparison to other FR II radio galaxies ($\langle \Gamma_\gamma \rangle = 2.38 \pm 0.05$). This observation can explain the detection of such a distant radio galaxy with the *Fermi*-LAT.

The 0.3–10 keV X-ray spectrum of TXS 1433+205 is steep ($\Gamma_X = 2.18 \pm 0.68$) in contrast to other FR II radio galaxies (Figure 3, top left panel) that typically exhibit flat X-ray spectra ($\Gamma_X < 2$, cf. Fukazawa et al. 2022). Such a steep falling X-ray spectrum is observed from the high synchrotron peaked BL Lac objects and is explained as the tail of the synchrotron emission (e.g., Abdo et al. 2011). If so, the corresponding inverse Compton peak is expected to be located at very high energies ($> 10 \text{ GeV}$) leading to the observation of a rising γ -ray spectrum ($\Gamma_\gamma < 2$). However, a soft γ -ray spectrum is detected

³ <https://tinyurl.com/9adwdtjf>

⁴ <https://tools.ssdsc.asi.it/SED>

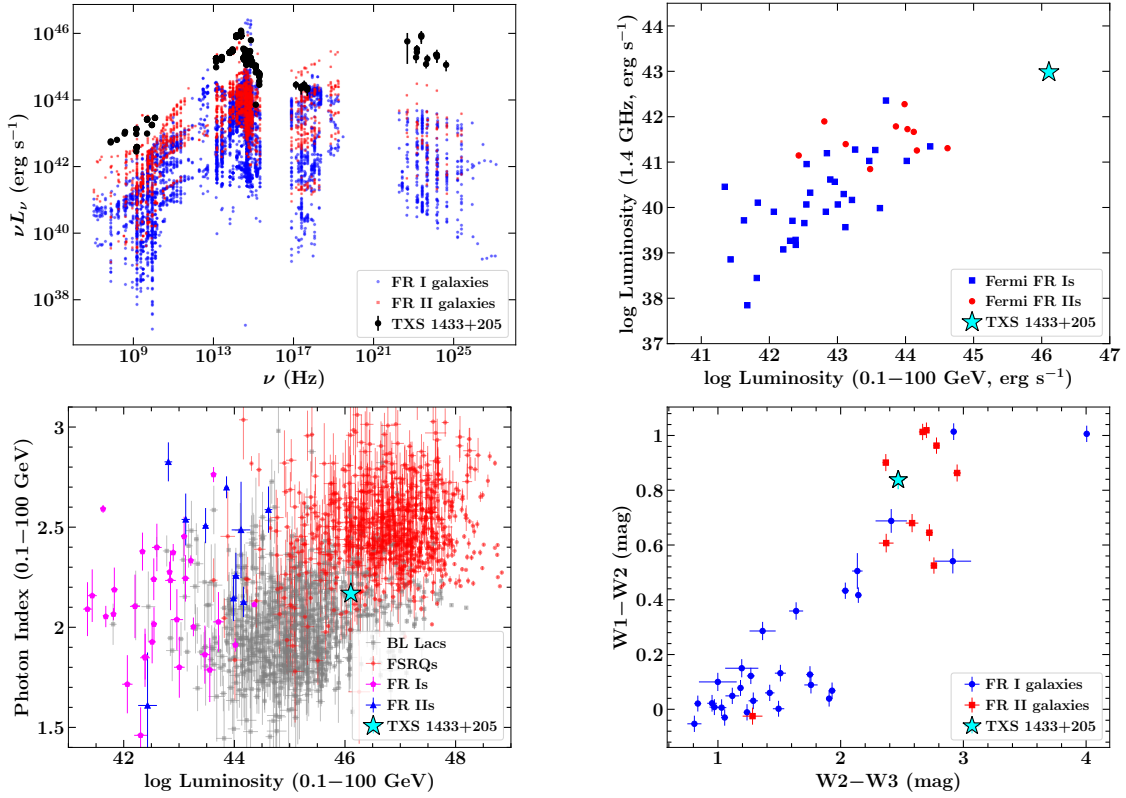


Figure 3. Top left: The multi-wavelength SED of TXS 1433+205 plotted along with other γ -ray detected FR I and II radio galaxies. Top right: This plot shows the radio luminosity as a function of the γ -ray luminosity for *Fermi*-LAT detected radio galaxies. Bottom left: The variation of the γ -ray spectral shape as a function of the γ -ray luminosity. Bottom right: The WISE colour diagram of γ -ray emitting radio galaxies.

from TXS 1433+205, thus challenging the conventional one-zone leptonic emission scenario. One possibility could be that there could be a non-negligible contribution from the X-ray emitting corona in the 0.3–10 keV band (e.g., [Grandi & Palumbo 2007](#)). Alternatively, more complex radiative processes, e.g., multi-zone structured jet ([Stawarz & Ostrowski 2002](#)), could be responsible for the observed peculiar X-ray and γ -ray spectra.

The infrared (IR)-to-ultraviolet SED of TXS 1433+205 shows a peak, likely due to the host galaxy, similar to that observed from other γ -ray detected radio galaxies. In the *Wide-field Infrared Survey Explorer* (WISE) colour-colour diagram, the source lies in a region mainly populated by γ -ray detected FR II radio galaxies (Figure 3, bottom right panel). Furthermore, to determine the contribution of the star-formation activities, we calculated the two-point spectral index $\alpha_{1.4}^{22}$ using the rest-frame flux densities at 22 μ m and 1.4 GHz, as follows:

$$\alpha_{1.4}^{22} = \frac{\log(F_{1.4 \text{ GHz}}/F_{22 \mu\text{m}})}{\log(\nu_{1.4 \text{ GHz}}/\nu_{22 \mu\text{m}})} \quad (1)$$

The typical value of $\alpha_{1.4}^{22}$ for jetted AGNs is > 0.2 (cf. [Caccianiga et al. 2015](#)). On the other hand, for sources with $\alpha_{1.4}^{22} < -0.25$, star-formation activities are expected to dominate the observed radio emission. Using NVSS and WISE data, we found $\alpha_{1.4}^{22} = 0.47$ for TXS 1433+205. This indicates the dominance of the jet emission in the observed radio and IR emission.

With both VLASS and *Fermi*-LAT operations active, along with other ongoing surveys, e.g., LOFAR and RACS, the identification of TXS 1433+205 as a γ -ray emitting radio galaxy can be considered

only as the tip of the iceberg (see also [Bruni et al. 2022](#)). Among the known γ -ray detected objects, the advent of the Square Kilometer Array will enable us to make deep images of these objects, and along with multi-wavelength data, may lead to the re-classification of several blazars or blazar candidates as radio galaxies. At the same time, the continuous monitoring of the γ -ray sky with the *Fermi*-LAT and optical spectroscopic followups will be crucial to detect faint γ -ray emitting AGN and constraining the high-energy radiation mechanism of these enigmatic cosmic radio sources.

ACKNOWLEDGEMENTS

We are grateful to the referee, Gabriele Bruni, for constructive criticism, which has helped improve the paper. VSP acknowledges a useful discussion with R. Srianand (IUCAA) and N. Gupta (IUCAA). We acknowledge the use of the SDSS and WISE data. Part of this work is based on archival data, software or online services provided by the Space Science Data Center - ASI. The National Radio Astronomy Observatory is a facility of the National Science Foundation operated under cooperative agreement by Associated Universities, Inc. CIRADA is funded by a grant from the Canada Foundation for Innovation 2017 Innovation Fund (Project 35999), as well as by the Provinces of Ontario, British Columbia, Alberta, Manitoba and Quebec.

DATA AVAILABILITY

All of the multi-wavelength data used in this article are publicly available at their respective data archives, e.g., VLASS cutout server (<http://cutouts.cirada.ca>).

REFERENCES

- Abdo A. A., et al., 2010, *ApJ*, 720, 912
 Abdo A. A., et al., 2011, *ApJ*, 736, 131
 Ahumada R., et al., 2020, *ApJS*, 249, 3
 Ajello M., et al., 2020, *ApJ*, 892, 105
 Best P. N., Heckman T. M., 2012, *MNRAS*, 421, 1569
 Bruni G., et al., 2022, *MNRAS*, 513, 886
 Buttiglione S., Capetti A., Celotti A., Axon D. J., Chiaberge M., Macchetto F. D., Sparks W. B., 2009, *A&A*, 495, 1033
 Caccianiga A., et al., 2015, *MNRAS*, 451, 1795
 Chiaro G., La Mura G., Domínguez A., Bisogni S., 2020, *Journal of High Energy Astrophysics*, 27, 77
 Condon J. J., Cotton W. D., Greisen E. W., Yin Q. F., Perley R. A., Taylor G. B., Broderick J. J., 1998, *AJ*, 115, 1693
 Dermer C. D., 1995, *ApJ*, 446, L63
 Fanaroff B. L., Riley J. M., 1974, *MNRAS*, 167, 31P
 Foschini L., et al., 2022, *Universe*, 8, 587
 Fukazawa Y., Matake H., Kayanoki T., Inoue Y., Finke J., 2022, *ApJ*, 931, 138
 Garrington S. T., Leahy J. P., Conway R. G., Laing R. A., 1988, *Nature*, 331, 147
 Garrington S. T., Conway R. G., Leahy J. P., 1991, *MNRAS*, 250, 171
 Grandi P., Palumbo G. G. C., 2007, *ApJ*, 659, 235
 Grandi P., Torresi E., Stanghellini C., 2012, *ApJ*, 751, L3
 Healey S. E., Romani R. W., Taylor G. B., Sadler E. M., Ricci R., Murphy T., Ulvestad J. S., Winn J. N., 2007, *ApJS*, 171, 61
 Hook I. M., McMahon R. G., Irwin M. J., Hazard C., 1996, *MNRAS*, 282, 1274
 Hooper D., 2016, *J. Cosmology Astropart. Phys.*, 2016, 002
 Intema H. T., Jagannathan P., Mooley K. P., Frail D. A., 2017, *A&A*, 598, A78
 Jackson N., Rawlings S., 1997, *MNRAS*, 286, 241
 Kataoka J., et al., 2011, *ApJ*, 740, 29
 Lacy M., et al., 2020, *PASP*, 132, 035001
 Laing R. A., 1988, *Nature*, 331, 149
 Landt H., Padovani P., Perlman E. S., Giommi P., 2004, *MNRAS*, 351, 83
 McConnell D., et al., 2020, *Publ. Astron. Soc. Australia*, 37, e048
 Pajdosz-Śmierciak U., Śmierciak B., Jamroz M., 2022, *MNRAS*, 514, 2122
 Paliya V. S., 2021, *ApJ*, 918, L39
 Petrov L., 2021, *AJ*, 161, 14
 Risaliti G., Salvati M., Marconi A., 2011, *MNRAS*, 411, 2223
 Saikia D. J., 2022, arXiv e-prints, p. arXiv:2206.05803
 Shimwell T. W., et al., 2022, *A&A*, 659, A1
 Stawarz Ł., Ostrowski M., 2002, *ApJ*, 578, 763
 Véron-Cetty M.-P., Véron P., 2010, *A&A*, 518, A10
 Wayth R. B., et al., 2015, *Publ. Astron. Soc. Australia*, 32, e025
 White R. L., Becker R. H., Helfand D. J., Gregg M. D., 1997, *ApJ*, 475, 479

APPENDIX A: VLBI IMAGE OF TXS 1433+205

Here we show the VLBI image of TXS 1433+205 taken from the list of VLBI Calibrators⁵ (cf. Petrov 2021).

This paper has been typeset from a $\text{\TeX}/\text{\LaTeX}$ file prepared by the author.

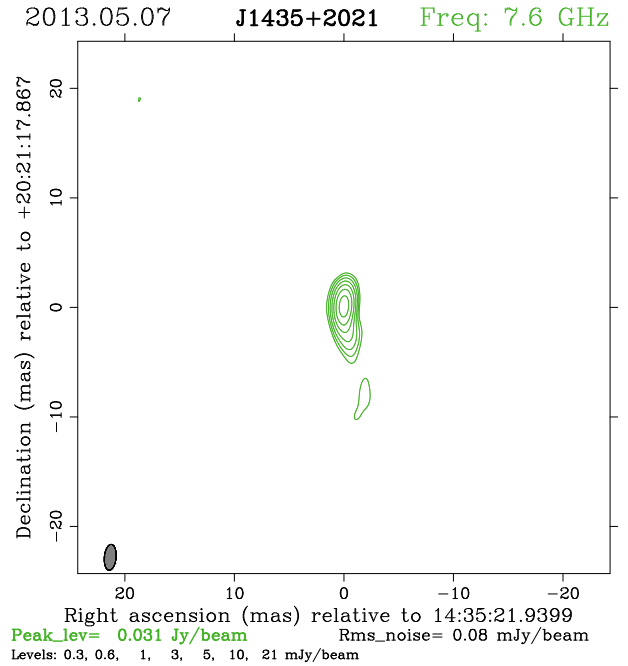


Figure A1. VLBI image of TXS 1433+205. Other information are provided in the figure.

⁵ <http://astrogeo.org/calib/search.html>